Journal of Innovative Optical Health Sciences
Vol. 2, No. 1 (2009) 117–122

World Scientific
www.worldscientific.com

DEVELOPMENT OF HIGH-SPEED SWEPT-SOURCE OPTICAL COHERENCE TOMOGRAPHY SYSTEM AT 1320 nm

TONG WU*, ZHIHUA DING*,‡, MINGHUI CHEN*, LEI XU*,
GUOHUA SHI† and YUDONG ZHANG†

*State Key Laboratory of Modern Optical Instrumentation
Zhejiang University, Hangzhou
Zhejiang 310027, China

†The Institute of Optics and Electronics
Chinese Academy of Sciences
Chengdu 610209, China
‡zh_ding@zju.edu.cn

A swept-source optical coherence tomography (SSOCT) system based on a high-speed scanning laser source at center wavelength of 1320 nm and scanning rate of 20 kHz is developed. The axial resolution is enhanced to 8.3 μm by reshaping the spectrum in frequency domain using a window function and a wave number calibration method based on a Mach-Zender Interferometer (MZI) integrated in the SSOCT system. The imaging speed and depth range are 0.04 s per frame and 3.9 mm, respectively. The peak sensitivity of the SSOCT system is calibrated to be 112 dB. With the developed SSOCT system, optical coherence tomography (OCT) images of human finger tissue are obtained which enable us to view the sweat duct (SD), stratum corneum (SC) and epidermis (ED), demonstrating the feasibility of the SSOCT system for *in vivo* biomedical imaging.

Keywords: Medical optics and biotechnology; optical coherence tomography; swept-source.

1. Introduction

Optical coherence tomography (OCT)[1] is an advanced biomedical imaging modality capable of providing micrometer scale cross-sectional images of biology tissue noninvasively. Because of its advantages of noninvasion, non-contact, and high resolution, OCT has found wide applications in biomedicine.[2–5]

Imaging speed is an important technical aspect of OCT. In the early OCT embodiment, which is called time-domain OCT (TDOCT), depth ranging is provided by linearly scanning the optical path length difference between the reference and the sample arm. The mechanical scanning results in the relatively slow imaging speed of TDOCT (approximately 2 kHz A-line rate).[6] Fercher *et al.* presents the Fourier domain OCT (FDOCT) based on spectral interferometry which has two embodiments, one is called spectral domain OCT (SDOCT), the other is called swept-source OCT (SSOCT).[7,8,10] FDOCT is the main approach to enhance imaging speed. The measurement speed of FDOCT is improved

‡Corresponding author.

dramatically by replacing the mechanical scanning with a wavelength-resolving detection scheme using a high-speed spectrometer or a high-speed tunable laser source in SDOCT and SSOCT, respectively. However, the state-of-the-art spectrometers are hampering further improvements with (1) the limited spectral resolution and wavelength range of the spectrometer, (2) the limited sensitivity and dynamic range of the CCD used in the spectrometer, and (3) higher device cost. Alternatively, SSOCT which uses a wavelength tunable laser and standard photo detector can also reach a high imaging speed without the limitations of the SDOCT. Another major advantage of FDOCT over TDOCT is its sensitivity, which has been proven both theoretically and experimentally.[9,11] However, FDOCT has its intrinsic drawbacks, that is, auto-correlation term and mirror term exist in the interference spectrum. Auto-correlation term exists at the zero optical length difference which results in the degradation of the signal-to-noise ratio (SNR) in the whole image. Recently, researchers have presented a series of methods to address these problems.[16–20]

Axial resolution is another important feature of OCT. The resolution of OCT is directly dependent on the bandwidth and spectrum shape of the light source. The non-Gaussian spectrum shape of the source will bring a lower axial resolution. Furthermore, the axial resolution of SSOCT system is affected by the acquisition mode of the interference spectrum signal. Because the wave number of the swept source is not linearly swept with time and the acquisition rate is constant with time, the sampled data of the interference spectrum signal is not equidistance in wave number space. A Fast Fourier transform of these data will cause a degradation of the axial resolution. So calibration of the sampled data[21] is necessary to ensure a high axial resolution. In recent publications, several approaches for frequency calibration of SSOCT have been demonstrated. These methods include the simultaneous frequency monitoring method,[13] the frequency even clock method,[14] data interpolation method and a fast calibration method based on nearest neighbor check algorithm.[15]

In this paper, an SSOCT system based on high-speed swept-source and Michelson interferometer is demonstrated. To prevent the degradation of axial resolution because of the non-Gaussian output spectrum of the swept source, a method based on window function to make the spectrum reshaping in the frequency domain is adopted. To ensure the system axial resolution, a wave number calibration method based on MZI integrated in the SSOCT system is introduced. To eliminate the auto-correlation term in the interference spectrum, both the common rejection of balanced detection and the software method of subtracting the mean value are used. Some high-speed optical coherence tomographic images of finger pad organism using the SSOCT system are obtained successfully.

2. System and Method

2.1. *System description*

A schematic of the SSOCT experimental set-up is shown in Fig. 1. A high-speed scanning laser source (HSL-2000, Santec Inc.) centered at 1320 nm with an FWHM (full-width at half-maximum) bandwidth of 107 nm is used as the light source. Ten percent of the output of the light source is introduced into the MZI through fiber coupler 1 with couple ratio of 10/90. The other part of the light passes through the 50/50 fiber coupler 2

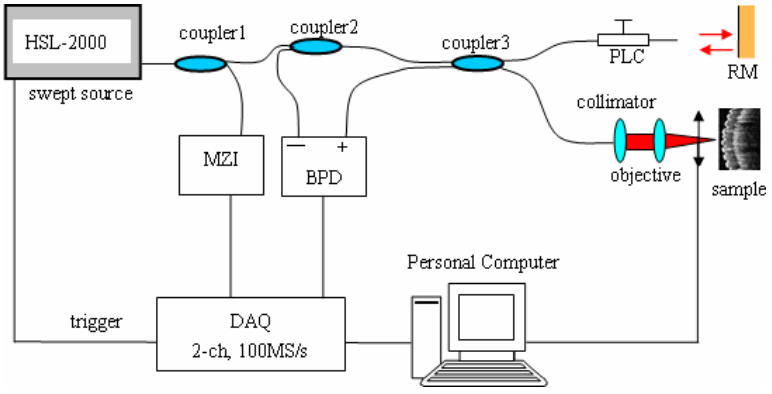

Fig. 1. Schematic of SSOCT system set-up. PLC: polarization controller. RM: reference mirror, MZI: Mach-Zender interferometer, BPD: balanced photo detector.

and 3, respectively, into the reference arm and sample arm. The sample arm is constituted by a fiber collimator, an achromatic lens of 40 mm focal length, and an electrical motorized translation stages. The reference arm has a polarization controller, a fiber collimator, focusing lens and a reference mirror (RM). After the recombination of the beams returning from sample and reference arm, the OCT interference spectrum signal is split into two beams by coupler 2 and 3. A balanced photo detector (BPD) detects the two beams of interference spectrum signal and converts the differential signal into voltage signal. One analog input channel of the data acquisition card (PCI-5122, NI) digitizes the OCT voltage signal. The output signal of the MZI is acquired by the second input channel of the DAQ card synchronously. The sampled data is transferred to the computer memory through the PCI bus. Post-processing of the sampled data involves background signal subtraction, spectrum reshaping in frequency domain, and interference spectrum signal calibration in wave number space, followed by Fourier transformation. The processed interference spectrum signal is Fourier transformed through a VC++ routine by a personal computer, yielding a complex signal with depth-resolved amplitude and phase information for the sample. The amplitude of the signal provides standard OCT information about the sample structure. After the image reconstruction process, the tomography images of biological tissue samples are displayed on a monitor.[12]

2.2. *System principle and parameters*

The interference spectrum signal can be given by Eq. (1):

$$I(k) = S(k)\left[1 + 2\int_0^\infty a(z)\cos(2knz)dz + \iint_0^\infty a(z) \times a(z')\exp[-i2kn(z-z')]dzdz'\right] \quad (1)$$

where $S(k)$ represents the intensity spectrum distribution of the light source, $a(z)$ the amplitude of the back scattering profile of the sample. $k(t) = 2\pi/\lambda(t)$ is the wave number which is varied in time by tuning of the laser. Here, $I(k)$ is called spectral density function. As shown in Fig. 2, the power spectral density is the Fourier transform of the corresponding auto-correlation function according to the Wiener-Khinchine theorem, i.e., the interference

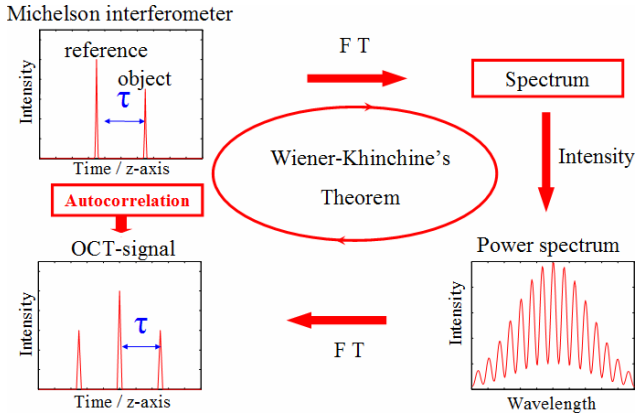

Fig. 2. Principle schematic of Fourier-domain optical coherence tomography.

spectrum signal is related to the reflection profile via the Fourier transform relation. A Fast Fourier transform (FFT) is performed from the sampled interference data to construct an axial scan. The result of FFT can be given by Eq. (2):

$$FT^{-1}[I(k)] = FT^{-1}[S(k)] \otimes \left\{[\delta(z)] + [a(z) + a(-z)] + \frac{1}{4}AC[a(z) + a(-z)]\right\} \quad (2)$$

In Eq. (2), auto-correlation term of the RM and the sample are the first and third term, respectively. These two terms are generally called auto-correlation term. The second term provides direct information on the positions of scattering layers in sample.

For a swept laser source with a Gaussian spectral envelope, the axial resolution of SSOCT system is given by[7]

$$\delta z = \frac{2\ln 2}{\pi}\frac{\lambda_0^2}{n\Delta\lambda} \quad (3)$$

where δz and $\Delta\lambda$ are the full-width at half-maximum (FWHM) of the spectral envelope, and n is the group refractive index of the sample. According to the practical system parameter, the theory axial resolution is 7.2 μm in air.

The maximum depth range achieved by a SSOCT system is given by[8]

$$\Delta z = \frac{\lambda_0^2}{4n\Delta\lambda}N_s \quad (4)$$

where λ_0 is the center wavelength and N_s is the number of samples within FWHM range $\Delta\lambda$ of the spectrum. According to the practical system parameter, the depth range is 3.9 mm in air.

2.3. *Interference spectrum calibration*

From Eq. (2), wave number k and axial coordinate z is a pair of Fourier transform. However, the sampled raw interference data is not equidistant in wave number space due to the non-linearity of the wave number scan in the swept source. Direct FFT from these raw data will cause a degradation of axial resolution. A MZI-based calibration method is adopted in the SSOCT system. According to the maximum value equation in interference fringe,

$$\Delta k \times d = 2\pi \tag{5}$$

where Δk is the wave number interval of the series of maximum points and d is the optical path length difference of two arms of the MZI. From Eq. (5), the wave number k of the maximum values is equally spaced at Δk when the optical path difference d is constant. When the MZI signal and OCT interference spectrum signal are acquired simultaneously, the maximum values of the MZI signal can calibrate the OCT interference spectrum and achieve a series of data equally distributed in wave number space.

2.4. *Spectrum reshaping*

The envelope shape of interference spectrum can affect the system resolution and side lobes.[22] Because of the imperfections in the characterization of the semiconductor optical amplifier (SOA) used in the light source, the laser source used in the system presents a non-Gaussian spectrum shape that may result in side lobes and broadened PSF. Reshaping of the spectrum can restrain side lobes and enhance axial resolution and image quality. A method based on window function is introduced in the SSOCT system to reshape the spectrum. The interference spectrum signal is multiplexed to an appropriate window function in the frequency domain to ensure system resolution and SNR. The window function is given in Eq. (6):

$$w(k) = \frac{1}{\Delta k}\left(\frac{1}{2} + \frac{1}{2}\cos\frac{\pi k}{\Delta k}\right) \tag{6}$$

where Δk is the wave number range of the laser source.

2.5. *Removal of the auto-correlation term*

Since the auto-correlation term exists at the zero optical path length difference where the best SNR can be achieved, to prevent from aliasing, the OCT signal should be removed away from this area. In our system, both hardware and software methods are adopted to make the best use of the zero optical path area. A BPD which can remove direct current signal common-mode noise is used to detect the OCT interference spectrum signal. Because of the system structure using two 50/50 couplers, the optical power is not equal at the two input ports of the balanced detector. For further subtraction of background signal, an average value of a sequence of A-Scans (i.e., a B-Scan) is calculated by software, the average value is subtracted from each A-line data to remove the remaining background signal.

3. Experiments and Results

To characterize the system performance, the axial point spread function was investigated by measuring the A-line profile of a partially reflecting mirror sample (95% reflectivity). In the experiment, a Hanning window function is used to reshape the spectrum in spectral domain. A Gaussian envelope of the interference spectrum can be obtained successfully through the spectrum reshaping method.

Based on MZI calibration and spectrum reshaping method, the system axial resolution is measured compared to that of direct FFT from non-calibrated data. The experiment result is shown in Fig. 3. The dashed line represents non-calibrated result whose FWHM value is broadened because of the raw data with non-equidistance wave number. From the solid line, we can get the practical axial resolution of the SSOCT system. The practical

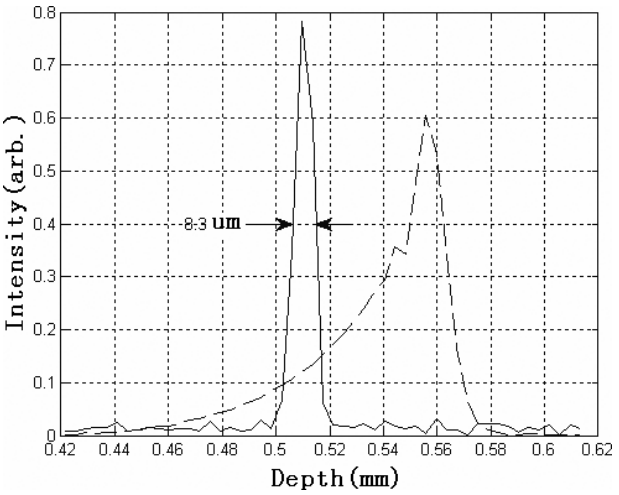

Fig. 3. A representative of point spread function measured using a mirror as sample.

resolution of 8.3 μm is approximate to the theoretical value with Gaussian spectrum of 7.2 μm based on the 107 nm FWHM bandwidth of the swept source. Small side lobes are the visible results from the interference calibration error and the departure of spectral shape of the light source from Gaussian.

To measure the practical depth range of the SSOCT system, a multilayer cover glass is used as the sample. The refractive index of the cover glass is 1.5, and according to Eq. (4), the depth range in glass is 2.44 mm. The experiment result is shown in Fig. 4. It can be seen that there are 14 layers in the image and the thickness of every cover glass is 0.175 mm, and then the practical depth range is 2.45 mm from calculation, which is in accordance with the theoretical value.

Figure 5 depicts an A-line profile of a -57 dB partial reflector placed as the sample in the SSOCT system. From the measured SNR of 55 dB, the sensitivity of the system is experimentally determined to be 112 dB.

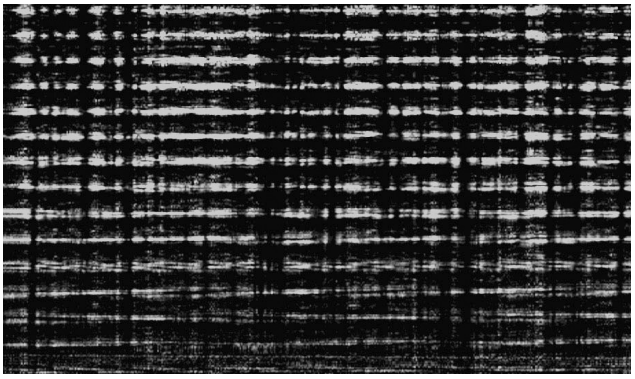

Fig. 4. Structural image of multilayer cover glass in OCT.

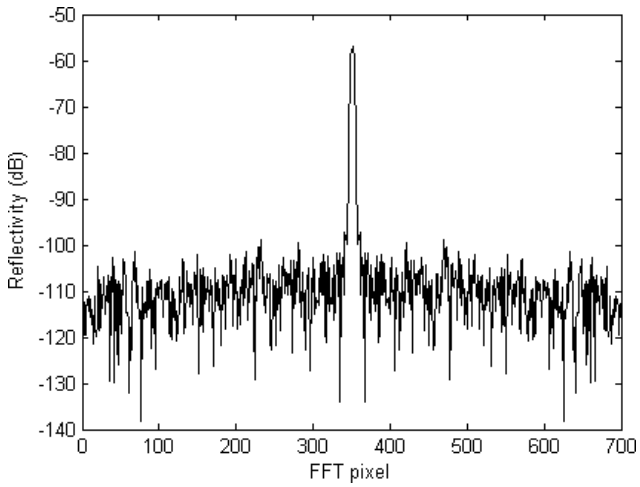

Fig. 5. Sensitivity measured with a partial reflector.

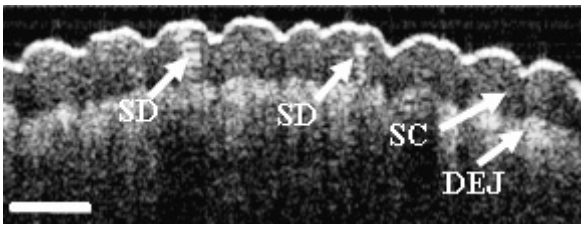

(a)

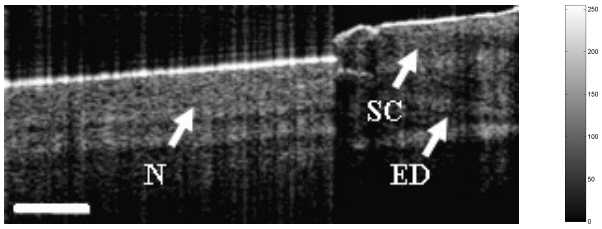

(b)

Fig. 6. Optical coherence tomography images of some different tissues taken by the SSOCT system.

To demonstrate the feasibility of the SSOCT system, some images of different biological tissues are presented in Fig. 6. The images shown are acquired with A-Scan rate of 20 kHz. The sampling rate was 100 M samples/s to acquire the images. The axial resolution is 8.3 μm in air, corresponding to 7 μm in tissue, and the lateral resolution is 12 μm. In the experiment, the auto-correlation term was suppressed sufficiently by dual balancing detection and background subtraction. Figure 6(a) shows an OCT image of the *in vivo* human finger skin. Figure 6(b) shows an OCT image of the *in vivo* human skin in the nail (N) fold region. Several structural features are visible in the images including finger print, sweat duct (SD), stratum corneum (SC), the dermal epidermal junction (DEJ), the epidermis (ED), and the nail (N). The white bar in these images represents 0.5 mm. The time needed to acquire data for one whole image is about 0.04 s. Meanwhile, some other OCT images of orange flesh and onion are acquired by the SSOCT system with evident tissue features.

4. Conclusion

In summary, an SSOCT system developed in the laboratory based on a high-speed scanning laser source is demonstrated. To improve the axial resolution, spectrum reshaping method and MZI calibration method are introduced in the SSOCT system. The achieved axial resolution of 8.3 μm is an approximate to the theoretical value. To make the

best utilization of the high SNR area of zero optical path length, both hardware method based on BPD and software subtraction method are employed. The OCT images of biological tissues are obtained, which demonstrate the feasibility of the SSOCT system.

Acknowledgments

This work was supported by the National High Technology Research and Development Program of China (2006AA02Z4E0, 2008AA02Z422) and Natural Science Foundation of China (60878057, 60478040).

References

1. Huang, D., Swanson, E. A. and Lin, C. P., "Optical coherence tomography," *Science* **254**(5035), 1178–1181 (1991).
2. Yu, X. F., Ding, Z. H., Chen, Y. H., Huang, L. N., Zhou, Z. M., Wu, L. and Liu, X., "Development of fiber-based optical coherence tomographic imaging system," *Acta Opt. Sinica.* **26**(2), 235–238 (2006).
3. Meng, J., Ding, Z.-H. and Zhou, L., "Axial super-resolution in optical coherence tomography," *Acta Photonica Sinica*, **37**(03), 533–536 (2008).
4. Yang, Y.-L., Ding, Z.-H., Yu, X.-F., Li, D. and Wang, L., "Dispersion Compensation in OCT System by Rapid Scanning Optical Delay Line," *Acta Photonica Sinica*, **37**(01), 21–24 (2008).
5. Wang, L., Ding, Z., Shi, G., Zhang, Y. D., Zhu, Y., Huang, G. and He, Z. A., "Fiber-Based optical coherence tomography imaging system with rapid scanning optical delay line as phase modulator," *Chinese J. Lasers.* **35**(03), 472–476 (2008).
6. Yun, S., Tearney, G. J., de Boer, J. F., Iftimia, N. and Bouma, B. E., "High-speed optical frequency-domain imaging," *Opt. Express*, **11**(22), 2953–2963 (2003).
7. Fercher, F., Hitzenberger, C. K., Kamp, G. and El-Zaiat, S. Y., "Measurement of intraocular distances by backscattering spectral interferometry," *Opt. Commun.* **117**, 443–448 (1995).
8. Hausler, G. and Lindner, M. W., "Coherence radar and spectral radar — new tools for dermatological diagnosis," *J. Biomed. Opt.* **3**, 21–31 (1998).
9. Leitgeb, R., Hitzenberger, C. and Fercher, A., "Performance of fourier domain vs. time domain optical coherence tomography," *Opt. Express*, **11**(8), 889–894 (2003).
10. Chinn, S. R., Swanson, E. A. and Fujimoto, J. G., "Optical coherence tomography using a frequency-tunable optical source," *Opt. Lett.* **22**(5), 340–342 (1997).
11. Choma, M., Sarunic, M., Yang, C. and Izatt, J., "Sensitivity advantage of swept source and Fourier domain optical coherence tomography," *Opt. Express*, **11**(18), 2183–2189 (2003).
12. Brinkmeyer, E. and Ulrich, R., "High-resolution OCDR in dispersive waveguide," *Electron. Lett.* **26**, 413–414 (1990).
13. Zhang, J., Rao, B., Wang, Q. and Chen, Z. P., Swept source fourier domain optical coherence tomography, in: *Optical Amplifiers and Their Applications/Coherent Optical Technologies and Applications* (Optical Society of America, 2006).
14. Choma, M. A., Hsu, K. and Izatt, J. A., "Swept source optical coherence tomography using an all-fiber 1300-nm ring laser source," *J. Biomed. Opt.* **10**, 044009 (2005).
15. Huber, R., Wojtkowski, M., Taira, K., Fujimoto, J. and Hsu, K., "Amplified, frequency swept lasers for frequency domain reflectometry and OCT imaging: design and scaling principles," *Opt. Express*, **13**(9), 3513–3528 (2005).
16. Wojtkowski, M., Kowalczyk, A., Leitgeb, R. and Fercher, A. F., "Full range complex spectral optical coherence tomography technique in eye imaging," *Opt. Lett.* **27**(16), 1415–1417 (2002).
17. Sarunic, M. V., Applegate, B. E. and Izatt, J. A., "Real-time quadrature projection complex conjugate resolved Fourier domain optical coherence tomography," *Opt. Lett.* **31**(16), 2426–2428 (2006).
18. Zhang, J., Nelson, J. S. and Chen, Z., "Removal of a mirror image and enhancement of the signal-to-noise ratio in Fourier-domain optical coherence tomography using an electro-optic phasemodulator," *Opt. Lett.* **30**(2), 147–149 (2005).
19. Yun, S., Tearney, G., de Boer, D. and Bouma, B., "Removing the depth-degeneracy in optical frequency domain imaging with frequency shifting," *Opt. Express.* **12**(20), 4822–4828 (2004).
20. Yasuno, Y., Makita, S., Endo, T., Aoki, G., Itoh, M. and Yatagai, T., "Simultaneous B-M-mode scanning method for real-time full-range Fourier domain optical coherence tomography," *Appl. Opt.* **45**(8), 1861–1865 (2006).
21. Huber, R., Wojtkowski, M., Fujimoto, J. G., Jiang, J. Y. and Cable, A. E., "Three-dimensional and C-mode OCT imaging with a compact, frequency swept laser source at 1300 nm," *Opt. Express.* **13**(26), 10523–10538 (2005).
22. Harris, F. J., "On the use of windows for harmonic analysis with the discrete fourier transform," *Proc. IEEE* **66**, 51–84.